Vertebrate Anatomy Morphology Palaeontology 11:133–150
ISSN 2292-1389

Computed tomographic investigation of a hatchling skull reveals ontogenetic changes in the dentition and occlusal surface morphology of Hadrosauridae (Dinosauria: Ornithischia)

Trystan M. Warnock-Juteau[1*], Michael J. Ryan[1,2], R. Timothy Patterson[1], Jordan C. Mallon[1,2]

[1]Ottawa-Carleton Geoscience Centre and Department of Earth Sciences, Carleton University, Ottawa, ON, K1S 5B6, Canada; trystanwarnockjuteau@cmail.carleton.ca; tim.patterson@carleton.ca; michaelj.ryan@carleton.ca

[2]Beaty Centre for Species Discovery and Palaeobiology Section, Canadian Museum of Nature, Ottawa, ON, K1P 6P4, Canada; jmallon@nature.ca

Abstract: CMN 8917 is a small, partial skull of a duck-billed dinosaur from the upper Campanian Dinosaur Park Formation in what is now Dinosaur Provincial Park, Alberta. It represents one of the few nestling-sized juvenile hadrosaurines known to date. Support for this phylogenetic placement includes a narial vestibule not enclosed within the premaxillary dorsal and lateral processes, the presence of an anterodorsal maxillary process, and a maxillary dorsal process that is longer anteroposteriorly than dorsoventrally. The skull also possesses tooth traits traditionally associated with lambeosaurines, such as secondary ridges on some maxillary and dentary tooth crowns, and denticulation on some maxillary tooth crowns. The occurrence of these features in a juvenile hadrosaurine suggests that they were modified during ontogeny, calling into question their taxonomic utility for identifying juvenile specimens. The dentary teeth of CMN 8917 are similar to those of many adult hadrosaurids in that they possess a concave occlusal surface with steeper lingual and shallower buccal wear zones. This differs from the occlusal surface morphology present in some other juvenile hadrosaurids, which suggests interspecific differences in dental battery development—possibly reflective of dietary differences—occurred during early ontogeny in some taxa.

INTRODUCTION

The Upper Cretaceous terrestrial fossil record in North America derives from some of the best studied and heavily sampled formations of the Mesozoic—including the Dinosaur Park (DPF) and Hell Creek formations (HCF)—which have yielded a wealth of fossil material and given researchers an unprecedented glimpse into the dinosaur-dominated ecosystems of that time (Currie 2005; Fastovsky et al. 2016). Most Upper Cretaceous terrestrial localities in North America were deposited by fluvial systems (Eberth et al. 2007; Brown et al. 2013; Fastovsky et al. 2016), that often generated hydraulic energies that biased against the preservation of small-bodied animals (Horner et al. 2011; Brown et al. 2013; Brown et al. 2022). Studies of modern bone assemblages have shown that large-bodied vertebrates are far more likely to be preserved than smaller individuals, even prior to fluvial transport, owing to differential weathering, scavenging, and trampling (Behrensmeyer et al. 1979). Given the addition of deep time and the potential effects of fluvial transport, it is expected that there would have been a strong bias against the preservation—and therefore the occurrence of—smaller carcasses in the terrestrial fossil record of Late Cretaceous North America.

As a result, small-bodied vertebrates are relatively rare occurrences in Upper Cretaceous deposits and are mostly known from incomplete or isolated remains, while larger-bodied animals are more common and often preserved as articulated skeletons (Eberth and Currie 2005; Horner et al. 2011; Brown et al. 2013; Brown et al. 2022). The

Published April 24, 2024
 submitted November 2, 2023; revisions received March 18, 2024; accepted April 1, 2024. Handling editor: Robert Holmes. DOI 10.18435/vamp29395

apparent size bias affects both small-bodied taxa and the juvenile forms of larger-bodied taxa; even juveniles of the largest and most abundant dinosaur groups, like hadrosaurids and ceratopsids, are relatively rare in the DPF and HCF (Eberth and Currie 2005; Horner et al. 2011; Brown et al. 2013; Brown et al. 2022). Regardless of the mechanisms behind the preservational bias against smaller-bodied vertebrates in these deposits, our understanding of Late Cretaceous North American ecosystems is likely hindered by an under sampling of small-bodied taxa and of juveniles of larger-bodied taxa (Brown et al. 2013; Benson 2018; Brown et al. 2022).

Chief among the inhabitants of the Late Cretaceous floodplains were the abundant Hadrosauridae, a clade that had evolved by the late Santonian (Bell and Brink 2013; Prieto-Márquez et al. 2016) and flourished until their disappearance during the K-Pg extinction event (Horner et al. 2004; Stubbs et al. 2019). Hadrosaurid fossils are known from Eurasia, Africa, the Americas, and Antarctica (Lull and Wright 1942; Case et al. 1998; Horner et al. 2004; Prieto-Márquez 2010; Stubbs et al. 2019; Longrich et al. 2021) suggesting a near-global distribution. The North American record of Hadrosauridae is especially impressive, with over 600 North American fossil localities having yielded hadrosaurid material (data from the Paleobiology Database (https://paleobiodb.org/)). As such, it is no surprise that hadrosaurids are among the most common dinosaur fossils from formations like the DPF (Eberth and Currie 2005; Brown et al. 2013). Hadrosauridae is divided into two major subfamilies: the crestless or solid-crested Hadrosaurinae (sensu Xing et al. 2017), and the hollow-crested Lambeosaurinae (Horner et al. 2004). While uncommon compared to adult and subadult specimens, juvenile material of both families is known (Waldman 1969; Dodson 1975; Horner and Currie 1994; Campione et al. 2013; Farke et al. 2013; Dewaele et al. 2015; Prieto-Márquez and Guenther 2018; Drysdale et al. 2019; Wosik et al. 2019; Takasaki et al. 2020; Mallon et al. 2022) and plays a key role in our understanding of hadrosaurid development. This juvenile material has been used to produce growth curves, study ontogenetic changes in morphology and potential ontogenetic shifts in diet, and support ideas of parental care in dinosaurs (Horner and Makela 1979; Horner et al. 2000; Evans 2010; Erickson and Zelenitsky 2014; Mallon et al. 2022; Wyenberg-Henzler et al. 2022). However, the almost complete lack of embryonic and nestling (sensu Hone et al. 2016) hadrosaurid specimens (Horner and Currie 1994; Dewaele et al. 2015; Prieto-Márquez and Guenther 2018; Wosik et al. 2019), has hampered our ability to understand the earlier stages of hadrosaurid ontogeny.

In 1955, Charles M. Sternberg described the partial skull of a small hadrosaurid from the upper Campanian rocks of what is now Dinosaur Provincial Park in Alberta, Canada. The specimen (CMN 8917) was collected from sandy clay deposits located 11 m above the Red Deer River and just under a kilometer southeast of the (now decommissioned) ferry in Steveville (Sternberg 1955). Based on Sternberg's account, the fossil originated from alluvial palaeochannel deposits of the lowermost 5 m of the Dinosaur Park Formation (P. J. Currie, pers. comm. to JCM, 12 July, 2023), and would have dated to approximately 76.4 Ma (Ramezani et al., 2022). Sternberg (1955) identified the specimen as a juvenile hadrosaurine, potentially related to *Gryposaurus*, though he refrained from assigning it to a specific genus. Sternberg's (1955) assignment was not based on currently recognized hadrosaurine synapomorphies. The rarity of juvenile material elevates the importance of this specimen. We therefore re-examined CMN 8917 using computed tomography, providing new insights into the animal's anatomy and into the early development of the hadrosaurid dental battery.

METHODOLOGY

CMN 8917 was submitted to X-ray computed tomography (CT) at the Transportation Safety Board of Canada in Ottawa, Ontario, Canada on April 21, 2022. The scan was performed using an X-View X5000 Industrial CT X-ray Inspection System at 180 kV and 88 μA using a microfocus xylon tube. The detector used was a 25 cm x 20 cm Varian 2520 with a pixel pitch of 127 μm. The resulting CT data consist of three image stacks in JPEG format with a 24-bit depth, representing slices through the frontal, sagittal, and transverse planes. The image stack representing the frontal plane consists of 1563 slices with a resolution of 1072 pixels x 656 pixels, that of the sagittal plane consists of 656 slices with a resolution of 1663 pixels x 1072 pixels, and that of the transverse plane consists of 1072 slices with a resolution of 1563 pixels x 656 pixels. All images have a pixel size of 51 μm x 51 μm, and a voxel size of 51 μm. The specimen was digitally segmented using the transverse image stack with the open-source software 3D Slicer 5.0.3. (https://www.slicer.org/) (Federov et al. 2012). The anatomy of CMN 8917 was documented using direct observation and segmentation of the CT data, and was compared to hadrosaurid material from the CMN, TMP, and to published descriptions of other hadrosaurid material (see Appendix 1: Table 1).

Institutional Abbreviations: AMNH, American Museum of Natural History, New York City, NY, USA; CMN, Canadian Museum of Nature, Ottawa, ON, Canada; DMNH, Perot Museum of Nature and Science, Dallas, TX, USA; MOR, Museum of the Rockies, Bozeman, MT, USA; MPC, Institute of Paleontology and Geology, Mongolian

Academy of Sciences, Ulaan Baatar, Mongolia; PU, Museum of Natural History, Princeton University, Princeton, NJ, USA; RAM, Raymond M. Alf Museum of Paleontology, Claremont, CA, USA; ROM, Royal Ontario Museum, Toronto, ON, Canada; TMP, Royal Tyrrell Museum of Palaeontology, Drumheller, AB, Canada; UCMP, University of California Museum of Paleontology, Berkeley, CA, USA; USNM, National Museum of Natural History, Washington, DC, USA; YPM, Peabody Museum of Natural History, Yale University, New Haven, CT, USA.

OSTEOLOGICAL DESCRIPTION AND COMPARISONS

The partial skull of CMN 8917 (Fig. 1) includes part of the left premaxilla, a nearly complete right maxilla with maxillary teeth, a partial left maxilla with some maxillary teeth, part of the right jugal, much of the right dentary including the dentary teeth, several left dentary teeth, and fragments of bone likely representing portions of the palate, though the latter are poorly preserved, making this identification uncertain. Some isolated material was collected alongside the skull, but is too weathered to be identified.

Premaxilla: A small portion of bone, labelled as the right premaxilla by Sternberg (1955), occurs anterolateral to the premaxillary shelf of the right maxilla; however, beyond its location in relation to other elements, the fragment preserves no identifying features. CT scans of CMN 8917 reveal that the left premaxilla is present, but poorly preserved, and as such, fine details of its morphology cannot be determined. The element (Fig. 2) is elongate, U-shaped, and flattened in the vertical plane. Viewed laterally, the posteroventral margin is sinusoidal, forming a subtle post-oral constriction which, when viewed dorsally, would have contributed to a spoon-shaped rather than a spatulate rostrum. This post-oral constriction is gradual (sensu Campione et al. 2013) as in *Prosaurolophus maximus* and *Gryposaurus* spp. (TMW-J, pers. obs.; Campione et al. 2013: fig. 1; Lowi-Merri and Evans 2020: fig. 3), and differs from the abrupt constriction seen in *Maiasaura peeblesorum*, *Brachylophosaurus canadensis* (Campione et al. 2013: fig. 1; Cuthbertson and Holmes 2010: fig. 3), and embryonic (TMP 1987.79.334), juvenile (CMN 2247, TMP 1994.385.1) and adult *Hypacrosaurus* spp. (CMN 2501) (TMW-J, pers. obs.; Horner and Currie 1994: fig. 21.16). At the center of the U-shaped arc of the premaxilla

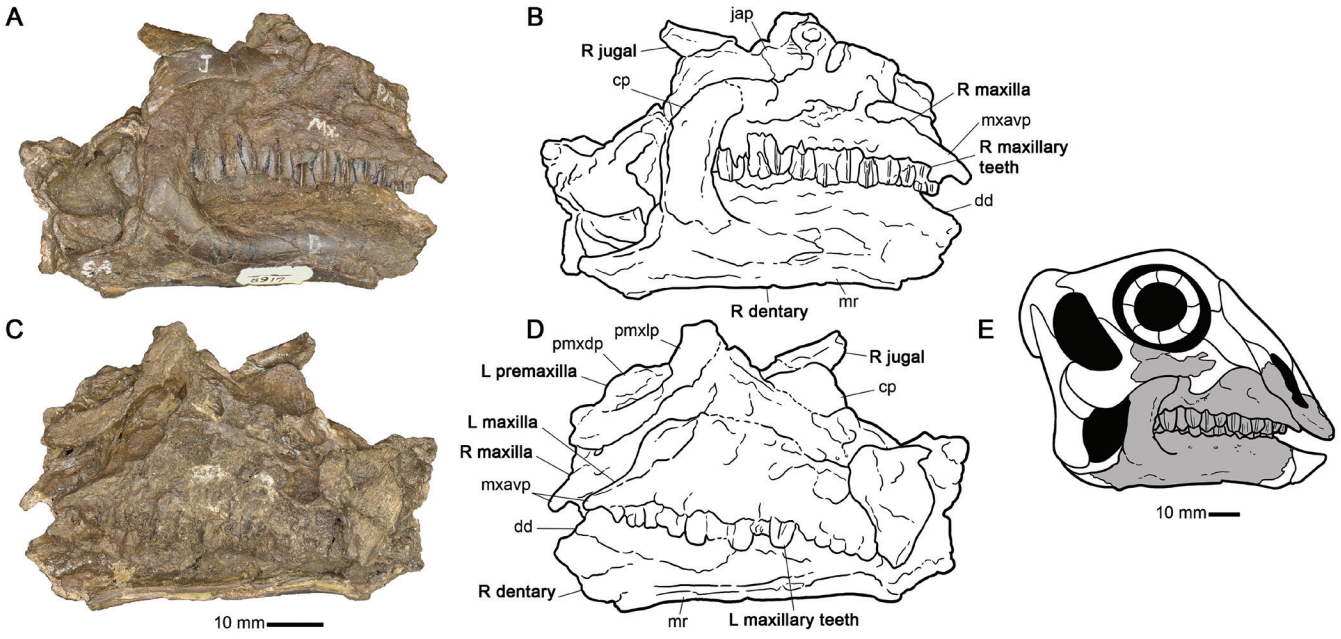

Figure 1. Juvenile hadrosaurine skull, CMN 8917. A, photograph of right lateral view; B, interpretive drawing of right lateral view; C, photograph of left lateral view; D, interpretive drawing of left lateral view; E, reconstruction of the skull in right lateral view: shaded regions represent portions of the skull preserved in CMN 8917, unshaded regions represent inferred skeletal elements based on reconstructions of nestling *Maiasaura peeblesorum* and embryonic *Hypacrosaurus stebingeri* (the left premaxilla of CMN 8917 was mirrored and fitted against the right maxilla for this reconstruction). Abbreviations: cp, coronoid process of the dentary; dd, diastema of the dentary; jap, jugal anterior process; L, left; mr, mandibular ramus; mxavp, maxillary anteroventral process; pmxdp, premaxillary dorsal process; pmxlp, premaxillary lateral process; R, right.

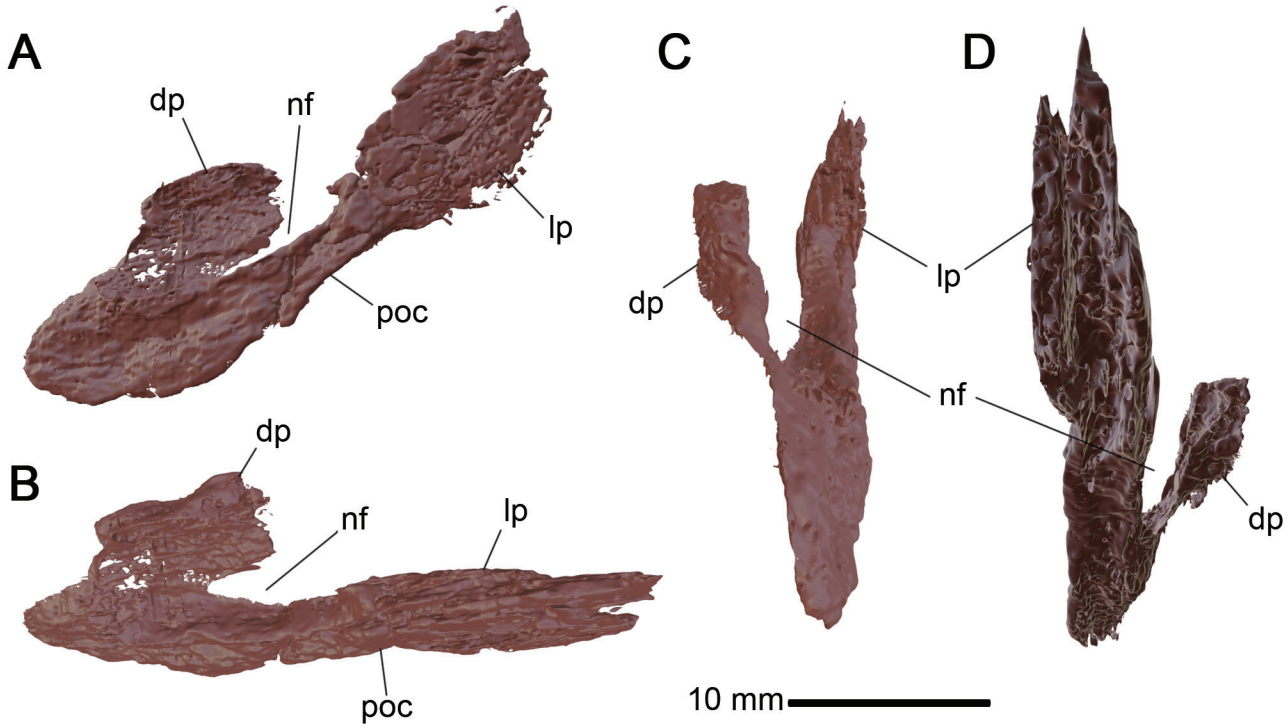

Figure 2. Left premaxilla of CMN 8917. A, lateral view; B, dorsal view; C, anterior view; D, posterior view. Abbreviations: dp, dorsal process; lp, lateral process; nf, narial foramen; poc, post-oral constriction.

lies a narrow, ovoid narial foramen, which is visible externally, as in hadrosaurines (Horner et al. 2004); in lambeosaurines, the dorsal and lateral processes of the premaxilla meet posteriorly, enclosing the narial vestibule (Horner et al. 2004).

Maxilla: The right maxilla (Fig. 3) is well preserved, though its lateral surface near the posterior half of the element is partly eroded. The left maxilla is poorly preserved. From the anterior tip of the anteroventral process to the posterior end of the element, the right maxilla measures 57.5 mm, although this is likely an underestimate, given the anteroventral process is not fully preserved. The maxilla is longer than that of embryonic *Hypacrosaurus stebingeri* (TMP 1987.79.336), which is approximately 45 mm long (Horner and Currie 1994: fig. 21.16), and those of nestling *Saurolophus angustirostris* (MPC-D100/764), reported as 20.6 mm long (Dewaele et al. 2015), but slightly shorter than those of large nestling *Maiasaura peeblesorum* (YPM-PU 22400), reported as 60 mm long (Horner et al. 2000; Prieto-Márquez and Guenther 2018). A portion of the premaxillary shelf of CMN 8917 is preserved along the anterodorsal margin of the maxilla; it is angled approximately 35° in relation to the anterior region of the alveolar margin, although given the poor preservation of the anteroventral region, this may be an underestimate. The angle of the premaxillary shelf appears to decrease during ontogeny in hadrosaurids (Horner 1992; Horner and Currie 1994; Prieto-Márquez and Guenther 2018), and thus may not be diagnostic in juvenile specimens. Though not fully preserved, an anterodorsal process—a feature present in hadrosaurines but absent in lambeosaurines (Horner et al. 2004)—projects anteromedially and slightly ventrally from the anterodorsal region of the maxilla. Posteroventral to the anterodorsal margin of the lateral surface of the maxilla, surrounded by a depression, is a small hole that extends mediolaterally to the medial surface. Although this was interpreted as a foramen by Sternberg (1955), the CT data show no evidence of cortical bone surrounding the opening, raising the possibility that it may have resulted from bioerosion.

The lateral surface of the maxilla between the premaxillary shelf and the jugal articulation surface appears to have formed an anteroposteriorly wide anterolateral promontory (sensu Xing et al. 2017), similar to that of kritosaurins (CMN 2278, CMN 8784, MOR 478-5-28-8-1, RAM 6797) (TMW-J, pers. obs.; Gates and Sampson 2007: fig. 7; Prieto-Márquez 2012: fig. 5), brachylophosaurins (CMN 8893, MOR 1071-8-13-98-559, PU 22504) (TMW-J, pers. obs.; Horner 1983: fig. 1; Freedman Fowler and Horner 2015: fig. 5), and saurolophins (CMN 2277, CMN 2870, CMN 8796, TMP 1983.64.3, TMP 2016.37.1). In the edmontosaurin *Edmontosaurus regalis* (CMM 2288, CMN 2289), the anterolateral promontory is more constricted than in the aforementioned tribes, and in many lambeosaurines, this region tapers dorsally, pinched between the premaxilla and jugal (CMN 2247, CMN 8503, CMN 8705, TMP

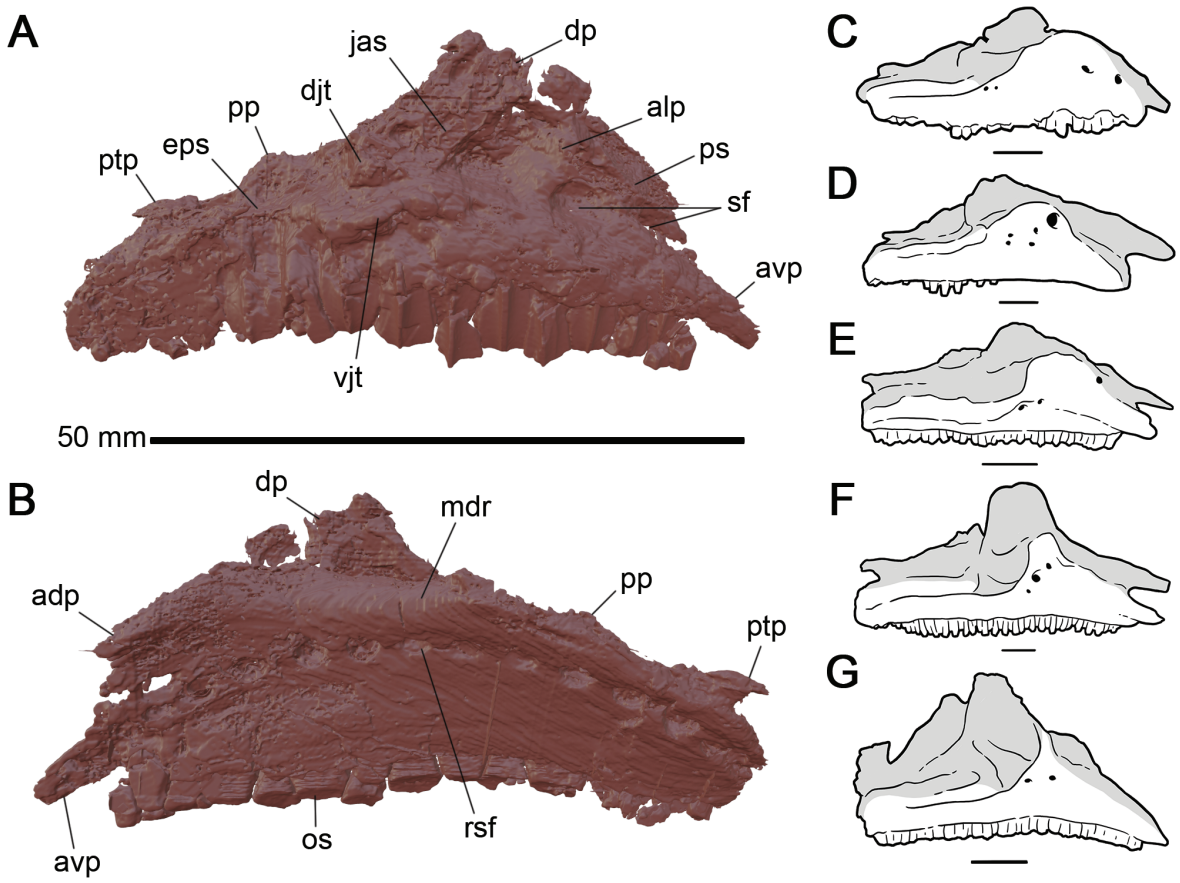

Figure 3. Right maxilla of CMN 8917 (A, B) compared with the maxillae of other taxa (C–G). A, CMN 8917 in lateral view; B, CMN 8917 in medial view; C, *Gryposaurus latidens* (MOR 478-5-28-1) (modified from Prieto-Márquez 2012); D, *Brachylophosaurus canadensis* (MOR 1071-8-13-98-559) (modified from Freedman Fowler and Horner 2015); E, *Prosaurolophus maximus* (TMP 2016.37.1); F, *Edmontosaurus regalis* (CMN 2289); G, *Corythosaurus casuarius* (CMN 8676). Shaded areas in illustrations represent articulation surfaces with other cranial elements. Abbreviations: adp, anterodorsal process; alp, anterolateral promontory; avp, anteroventral process; djt, dorsal jugal tubercle; dp, dorsal process; eps, ectopterygoid shelf; jas, jugal articulation surface; mdr, mediodorsal ridge; os, occlusal surface; pp, palatine process; ptp, pterygoid process; rsf, row of special foramina; sf, Sternberg's proposed foramina; vjt, ventral jugal tubercle. Scale bars are all 50 mm.

1966.4.1, TMP 1994.385.1, TMP 1994.666.80, ROM 702) (TMW-J, pers. obs.; Wagner and Lehman 2009: fig. 3; Evans 2010: fig. 6).

Two large depressions occur on the surface of the anterolateral promontory; the first located anterior to the mid-point between the premaxillary shelf and the jugal contact surface, and the second posterodorsal to the first. Despite the anterior-most depression matching the location of the anterior-most maxillary foramen in some kritosaurins (CMN 2278, MOR 478-5-28-8-1, RAM 6797) (TMW-J, pers. obs.; Gates and Sampson 2007: fig. 7; Prieto-Márquez 2012: fig. 5) and *B. canadensis* (CMN 8893, MOR 1071-8-13-98-559) (TMW-J, pers. obs.; Freedman Fowler and Horner 2015: fig. 5 E), as noted by Sternberg (1955), there is no evidence in the CT data that either depression communicated with a foramen.

A flat, textured jugal articulation surface occurs near the mid-length of the maxilla, with its anteroventral margin being subtly sinusoidal and angled anterodorsally. The jugal articulation surface transitions dorsally into a subtriangular dorsal process, which tapers posterodorsally. The dorsal process is longer anteroposteriorly than dorsoventrally, as in hadrosaurines; in lambeosaurines, the dorsal process is longer dorsoventrally (Horner et al. 2004). The apex of the dorsal process is located anterior to the anteroposterior mid-length of the maxilla, as in other immature hadrosaurids (Horner and Currie 1994; Prieto-Márquez and Guenther 2018; Takasaki et al. 2020). The ventral rim of the jugal articulation is bordered by the laterally projecting ventral jugal tubercle, which originates in line with the apex of the dorsal process and continues posteroventrally. Anteroventral to the ventral jugal tubercle is an arcuate row of four small foramina extending anterodorsally, which

may have housed vasculature and/or the maxillary branches of the trigeminal nerve (Galton 1973; Horner et al. 2004). A bulbous dorsal jugal tubercle occurs dorsomedial to the ventral jugal tubercle. Behind the dorsal jugal tubercle, the ectopterygoid shelf extends posteroventrally towards the posterior end of the maxilla at an angle of approximately 7° in relation to the alveolar margin. Lateral to the ectopterygoid shelf the maxilla is eroded, so little of the ectopterygoid ridge is preserved. Medial to the ectopterygoid shelf is a small, mediolaterally thin, triangular palatine process, which appears incomplete. Located posterior to the palatine process, the pterygoid process projects posteriorly, tapering to form a conical spur, posterior to which the maxilla ends in a blunt terminus.

In medial view, a dorsally arcuate row of special foramina (sensu Edmund 1957), located dorsal to the dorsoventral midline of the maxilla, marks the base of the maxillary tooth families. In life, the maxilla would likely have possessed one foramen per tooth family (Horner et al. 2004), but only 13 foramina are preserved in the right maxilla of CMN 8917 despite it possessing 15 tooth families. The dorsomedial margin of the element is laterally expanded, forming a prominent mediodorsal ridge (sensu Prieto-Márquez 2012), which appears to have extended from the posterior end of the element to the medial side of the anterodorsal process.

Jugal: The right jugal (Fig. 4) is preserved, but missing much of the anterior and postorbital processes as well as the region posterior to and including the infratemporal fenestra. The shape of the jugal articulation surface on the maxilla indicates that the anteroventral margin of the of the anterior process of the jugal was subtly sinusoidal and anterodorsally inclined, reminiscent of the triangular anterior process of some kritosaurins (CMN 2278, MOR 478-5-28-8-1) (TMW-J, pers. obs.; Prieto-Márquez 2012: fig. 5) and brachylophosaurins (CMN 8893, PU 22405) (TMW-J, pers. obs.; Horner 1983: figs. 1, 2). In *Edmontosaurus regalis* (CMN 2289) and *Prosaurolophus maximus* (CMN 2277, CMN 2870, TMP 2016.37.1), the anteroventral margin arcs dorsally, producing a much more pronounced S-shape than in CMN 8917, while in lambeosaurines the jugal anterior process is rounded or D-shaped (CMN 2247, CMN 8501, CMN 8503, CMN 8703, CMN 8704, ROM 702, TMP 1966.4.1, TMP 1994.385.1) (TMW-J, pers. obs.; Evans 2010: fig. 2, 6). In *G. notabilis* and many lambeosaurines, the shape of the jugal anterior process changed minimally throughout ontogeny (Waldman 1969; Evans 2010), although this is not the case in *M. peeblesorum*, where it changes from a rounded process in nestlings (Prieto-Márquez and Guenther 2018) to a triangular process in adults (Horner 1983), or in the juvenile *Parasaurolophus* sp. RAM 14000, where the process is triangular (Farke et al. 2013), more akin to the morphology seen in many hadrosaurines. Given potential ontogenetic variability in this feature, the shape of the jugal anterior process may be of questionable taxonomic utility when dealing with juvenile material.

On the medial surface of the jugal, the maxillary contact surface is flat, surrounded by a thin rim of bone on the posterodorsal and posteroventral margins of the contact surface, the former likely representing the palatine contact surface. The dorsal surface of the jugal neck and the preserved portion of the postorbital process form a wide orbital margin,

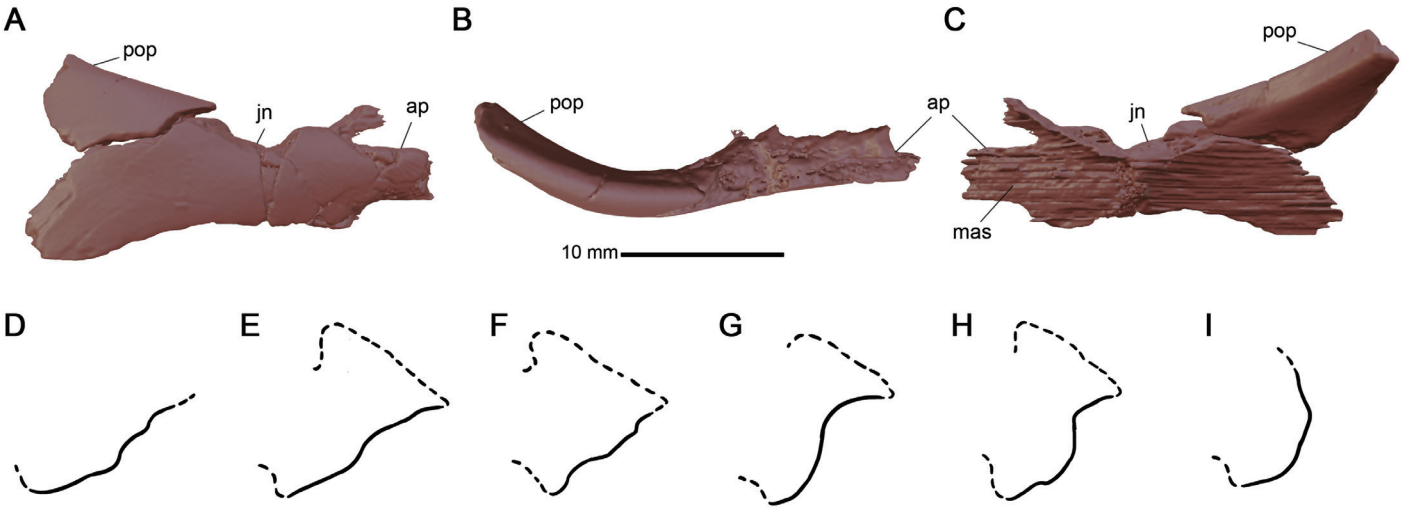

Figure 4. Right jugal of CMN 8917 (A–C) and illustrations of the anteroventral margin of the jugal anterior process in CMN 8917 and other taxa (D–I). The jugal of CMN 8917 in A, lateral view; B, dorsal view; C, medial view; illustrations of the anteroventral margin of the jugal anterior process in right lateral view (D–I) of D, CMN 8917 (reconstructed based on the anteroventral margin of the jugal contact surface on the maxilla); E, *Gryposaurus notabilis* (CMN 2278); F, *Brachylophosaurus canadensis* (CMN 8893); G, *Prosaurolophus maximus* (TMP 2016.37.1); H, *Edmontosaurus regalis* (CMN 2288); I, *Hypacrosaurus stebingeri* (TMP 1994.385.1). Abbreviations: ap, anterior process; jn, jugal neck; mas, maxilla articulation surface; pop, postorbital process.

as in other early-stage hadrosaurids (Horner and Currie 1994; Dewaele et al. 2015; Prieto-Márquez and Guenther 2018).

Dentary: The right dentary (Fig. 5) is well preserved, but much of the region anterior to the dental battery is missing. A small portion of the diastema is present, and dips anteroventrally at an angle of approximately 154° in relation to the long axis of the mandibular ramus. In lateral view, the ventral margin of the mandibular ramus is slightly bowed, reaching its lateral-most extent anterior to the base of the coronoid process, as in *Gryposaurus* spp. (CMN 2278, AMNH FARB 5465) (TMW-J, pers. obs.; Prieto-Márquez 2012: fig. 8) and *E. regalis* (CMN 2289), although the bowing is more pronounced in the latter taxon. In both adult and juvenile specimens of *P. maximus* the bowing is more pronounced and may reach its apex anterior (CMN 2870, TMP 1983.64.3, TMP 1984.1.1, TMP 2016.37.1) or ventral (ROM 787) to the coronoid process (TMW-J, pers. obs.; McGarrity et al. 2013: figs. 5, 7, 12). The bowing is more pronounced and occurs ventral to the coronoid process in *B. canadensis* (CMN 8893) and many lambeosaurines including *Lambeosaurus magnicristatus* (CMN 8705), juvenile *Corythosaurus casuarius* (CMN 36141), and embryonic (Horner and Currie 1994: fig. 21.23), juvenile, and subadult *Hypacrosaurus* spp. (CMN 2247, TMP 1988.151.88, TMP 1994.385.1). The ventral margin of the dentary of CMN 8917, anterior to the ventral bowing, deflects subtly anteroventrally. This anterior deflection decreases over ontogeny in some hadrosaurines (Takasaki et al. 2020) and is generally more pronounced in lambeosaurines (TMW-J, pers. obs.; Sternberg 1955; Horner et al. 2004).

The lateral surface of the mandibular ramus of CMN 8917 bows outward, reaching its lateral-most extent ventral to the dorsoventral mid-height of the mandibular ramus (Fig. 6), dorsal to which its flat surface bears several small foramina which may have housed nerves or blood vessels (Galton 1973). The lateral-most point of this bowing occurs ventral to the mid-height of the mandibular ramus in many juvenile (TMP 2016.37.1, ROM 1939) (TMW-J, pers. obs.; Mallon et al. 2022: fig. 9) and adult hadrosaurines (AMNH FARB 5465, AMNH 5799, CMN 2277,

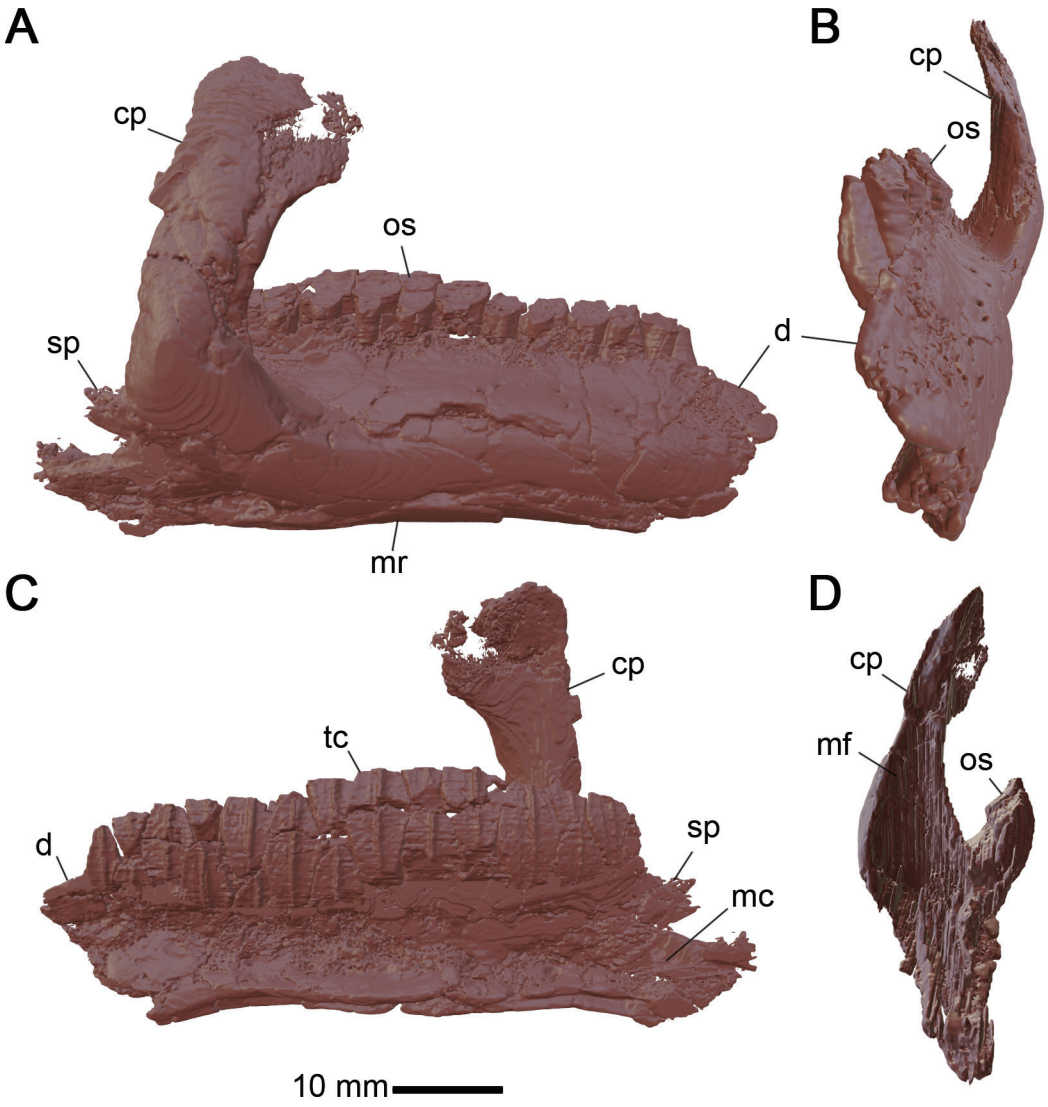

Figure 5. Right dentary of CMN 8917. A, lateral view; B, anterior view; C, medial view; D, posterior view. Abbreviations: cp, coronoid process; d, diastema; mc, Meckelian canal; mf, Meckelian fossa; mr, mandibular ramus; os, occlusal surface; sp, splenial process; tc, tooth crown.

CMN 2278, CMN 2289, CMN 2870, CMN 8893, ROM 787, TMP 1984.1.1, USNM 8629) (TMW-J, pers. obs.; Cuthbertson and Holmes 2010: fig. 5; McGarrity et al. 2013: figs, 5, 7, 9, 12; Prieto-Márquez 2012: fig. 8; Prieto-Márquez 2014: fig. 1, 17), although an adult specimen of *Saurolophus osborni* (CMN 8796) indicates that this is not always the case. Although the dentaries of known hadrosaurine nestlings are poorly preserved, this prominence occurs more ventrally in some *M. peeblesorum* specimens (YPM-PU 22400) (Prieto-Márquez and Guenther 2018: fig. 4). In many juvenile (CMN 36141, TMP 1988.151.88, TMP 1994.385.1, RAM 14000) (TMW-J, pers. obs.; Farke et al. 2013: fig. 7) and some adult lambeosaurines (CMN 8503, CMN 8673, CMN 8704, TMP 1966.4.1), the lateral bowing extends dorsally to or above the dorsoventral mid-height of the mandibular ramus, although in other adult lambeosaurines (CMN 8501, CMN 8703, CMN 8705) it occurs more ventrally. Regardless of the variation present in adult lambeosaurines, in juvenile lambeosaurines the maximum bowing appears to be located consistently at or dorsal to the mid-height of the ramus, while in juvenile and adult hadrosaurines it tends to be located more ventrally.

The large coronoid process of the dentary projects anterodorsally at an angle of 16° relative to the vertical. The coronoid process is angled anterodorsally in adult (Horner et al. 2004), and some nestling (UCMP 235860) (Wosik et al. 2019: fig. 2) and juvenile hadrosaurids (TMP 2016.37.1, TMP 1988.151.88, TMP 1994.385.1) (TMW-J, pers. obs.), but is angled vertically or posterodorsally in embryonic (TMP 1987.79.266, TMP 1989.79.52) (Horner and Currie 1994: figs. 21.4 C, 21.23) and some nestling hadrosaurids (MPC-D100/764, YPM-PU 22400) (Dewaele et al. 2015; Prieto-Márquez and Guenther 2018: fig. 4).

The base of the coronoid process in CMN 8917 is separated from the dental battery by a dorsally concave shelf, above which the coronoid extends dorsomedially to rest beneath the jugal. The coronoid process becomes mediolaterally compressed towards its dorsal end, with the apex of the process being thin and partially broken. The dorsal margin of the coronoid process, when viewed laterally, is subtrapezoidal and expanded anteriorly. The dorsal margin of the coronoid process is angled anteroventrally as in *Kritosaurus navajovius* (AMNH 5799) (Prieto-Márquez 2014: fig. 14), *Prosaurolophus* spp. (TMP 2016.37.1, MOR 447-8-11-7-2) (TMW-J, pers. obs.; Horner 1992: plate 34), and *E. regalis* (CMN 2289), although juvenile edmontosaurin specimens appear to possess more rounded dorsal margins (Takasaki et al. 2020). Embryonic (TMP 1987.79.266), juvenile, and subadult (TMP 1988.151.88, TMP 1994.385.1) *H. stebingeri* specimens also possess an anteroventrally inclined dorsal margin (TMW-J, pers. obs.; Horner and Currie 1994: fig. 21.23), which suggests that the shape of the apex of the coronoid process is conserved throughout ontogeny in some taxa. The apex of the coronoid process of CMN 8917 differs from those of *G. latidens* (AMNH FARB 5465) and *B. canadensis* (CMN 8893), which have horizontal dorsal margins (Cuthbertson and Holmes 2010: fig. 5; Prieto-Márquez 2012: fig. 8). In some *B. canadensis* (CMN 8893) and *E. regalis* (CMN 2289) dentaries, a short, tapering spur projects from the posterodorsal edge of the coronoid process, although this is not always preserved (Cuthbertson and Holmes 2010: fig. 5; Xing et al. 2017: fig. 16). Viewed posteriorly, the coronoid process of CMN 8917 possesses a large, lens-shaped Meckelian fossa.

The mandibular ramus extends posterior to the base of the coronoid, tapering to form a dorsally concave triangular process that would have cupped the surangular dorsomed-

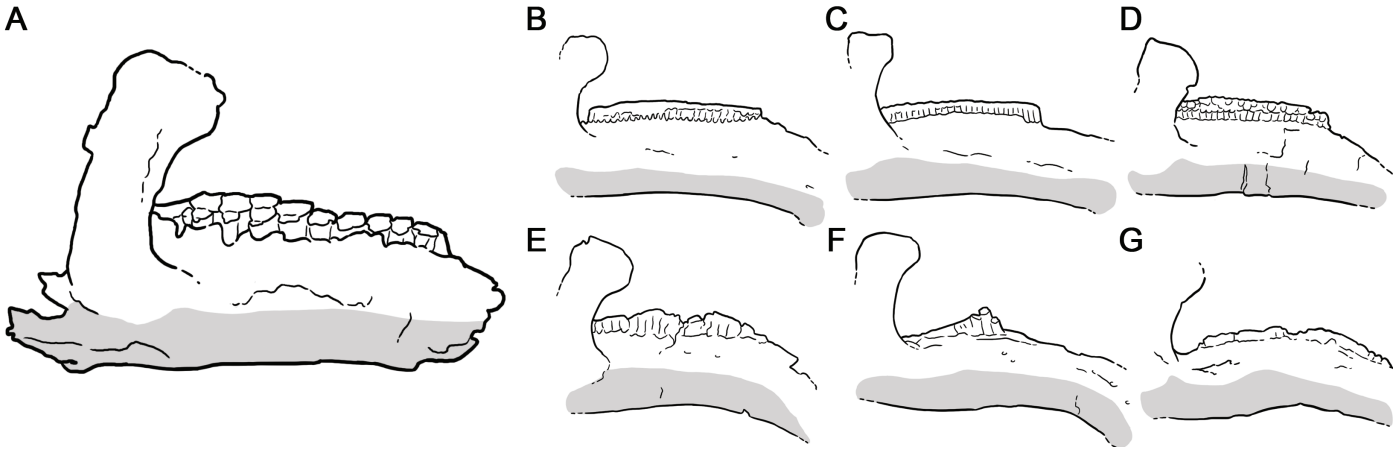

Figure 6. Mandibular ramus comparisons. A, CMN 8917; B, G*ryposaurus latidens* (AMNH FARB 5465) (modified from Prieto-Márquez 2012); C, *Brachylophosaurus canadensis* (CMN 8893); D, juvenile *Prosaurolophus maximus* (TMP 2016.37.1); E, juvenile *Hypacrosaurus stebingeri* (TMP 1994.385.1); F, juvenile *Corythosaurus casuarius* (CMN 36141); G, *Corythosaurus casuarius* (CMN 8503). Shaded areas indicate portions of the mandibular ramus ventral to the point of maximum lateral curvature. Specimen illustrations are not to scale.

ially. A portion of bone inset from the ventral border of the posteroventral section of the dentary may represent a part of the surangular, as suggested by Sternberg (1955); however, this region is fragmented, making it difficult to confirm whether this bone represents a separate element or a displaced portion of the dentary.

The dental lamina is missing, fully exposing the medial surfaces of the dentary teeth. Posteroventral to the dental battery, when viewing the dentary medially, there is a posteriorly tapering, mediolaterally thin triangular splenial process, below which the wedge-shaped Meckelian canal tapers anteriorly.

Maxillary Dentition: The teeth of the right maxilla (Fig. 7) are well preserved; some of the teeth of the left maxilla are present, but poorly preserved. There are 15 tooth families present in the right maxilla, more than the 13 mentioned in Sternberg's (1955) original description, but significantly fewer than in adult hadrosaurids (Horner et al. 2004). Up to 15 tooth families occur in nestling *Maiasaura peeblesorum* (Prieto-Márquez and Guenther 2018), and approximately 12 and 20 in embryonic and nestling *Hypacrosaurus stebingeri*, respectively (Horner and Currie 1994). The maxilla of CMN 8917 contains two teeth per alveolus, except in the first and last alveoli, which contain one tooth each. A single tooth contributes to the occlusal surface of any given tooth family, while in nestling *M. peeblesorum* maxillae there can be up to two functional maxillary teeth per alveolus (Prieto-Márquez and Guenther 2018). The occlusal surfaces on the teeth of CMN 8917 are planar or subtly concave and angled between 30° and 40° from the horizontal. As in other hadrosaurids (Weishampel 1984; Cuthbertson et al. 2012), the maxillary tooth rows are longer than the dentary tooth rows.

The maxillary tooth crowns are lanceolate, with a prominent, straight dorsoventral primary ridge present on the labial surface, as in other hadrosaurids (Horner et al. 2004). The ratio between dorsoventral and mesiodistal length in an unworn tooth crown near the mid-point of the maxilla is 1.6, though the height-to-width ratio of hadrosaurid tooth crowns appears to increase over ontogeny (Erickson and Zelenitsky 2014; Fondevilla et al. 2018), making it of little diagnostic use when dealing with juvenile specimens. In CMN 8917, the primary ridges are generally located distal (sensu Smith and Dodson 2003) to the mesiodistal mid-length of the tooth crowns, though in a few instances the primary ridge occurs near the mesiodistal mid-length of the crown. The fifth maxillary tooth from anterior has a prominent secondary ridge located mesial to the primary ridge. A couple of the maxillary teeth possess knobby denticles on the mesial and distal apical margins of the tooth crown, which are only visible in the CT images. Denticulated margins are generally better developed in lambeosaurines (Horner et al. 2004), although prominent denticles are present in *Gryposaurus latidens* (AMNH FARB

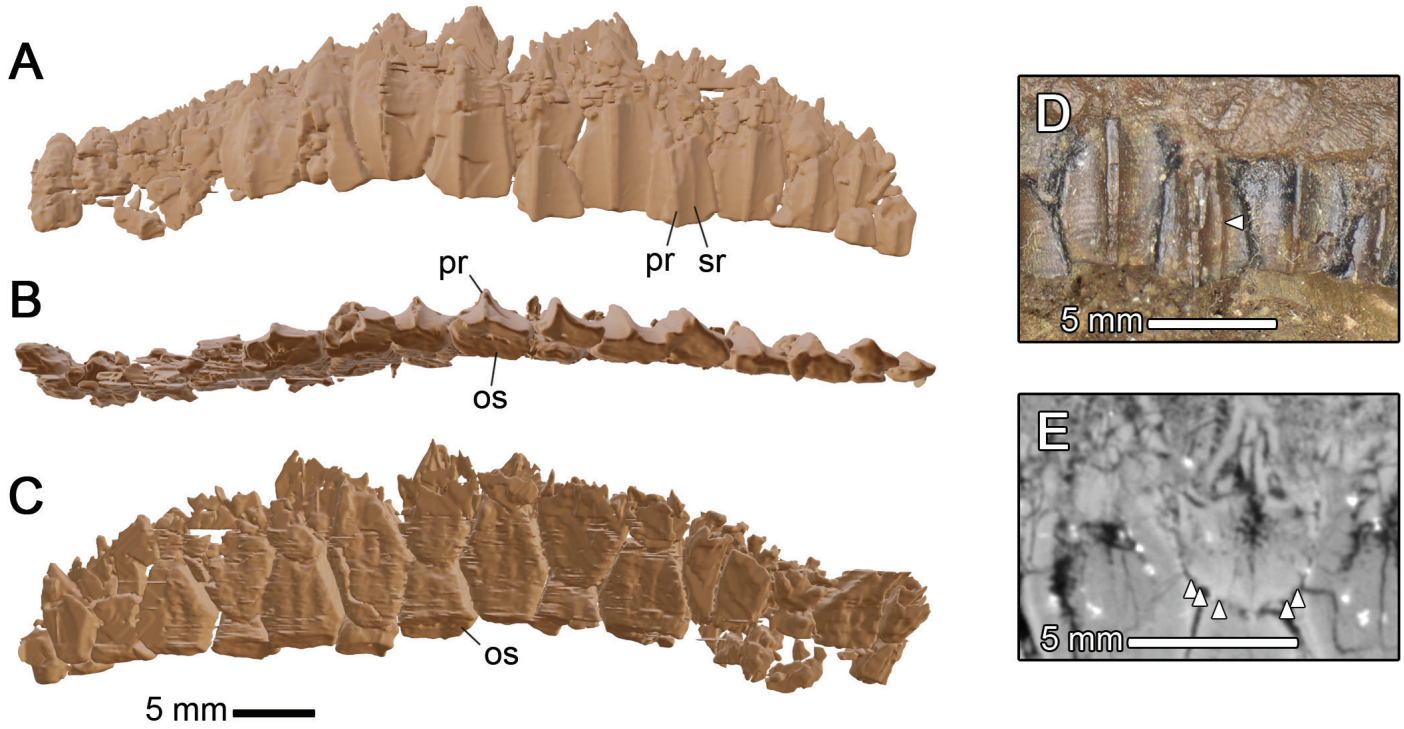

Figure 7. Right maxillary dentition of CMN 8917. Maxillary tooth rows (A–C) in A, labial view; B, apical view; C, lingual view; D, labial view of the fifth maxillary tooth from anterior, with arrow pointing to the secondary ridge; E, sagittal cross-section of maxillary teeth, with arrows pointing to denticles. Abbreviations: os, occlusal surface; pr, primary ridge; sr, secondary ridge.

5465) (Prieto-Márquez 2012), and more diminutive ones in *Kritosaurus navajovius* (AMNH 5799) (Prieto-Márquez 2014) and *M. peeblesorum* (Prieto-Márquez and Guenther 2018). Denticulation occurs in embryonic and nestling *Hypacrosaurus stebingeri* specimens, but is more prominent in the former (Horner and Currie 1994). Both secondary ridges and prominent denticulation on tooth crowns appear to vary ontogenetically in some taxa (Horner and Currie 1994; Mallon et al. 2022) and may be plesiomorphic, given their occurrence in non-hadrosaurid iguanodontians (Horner et al. 2004).

Dentary Dentition: The right dentary teeth (Fig. 8) are well preserved; a few of the left dentary teeth are present, but heavily eroded and preserve little detail. There are 14 tooth families present in the right dentary, more than the 10–12 reported in nestling *Maiasaura peeblesorum* (Prieto-Márquez and Guenther 2018) or 8–11 reported in embryonic *Hypacrosaurus stebingeri* (Horner and Currie 1994). In contrast, nestling specimens of *H. stebingeri* reportedly have up to 21 tooth families (Horner and Currie 1994). The dentary of CMN 8917 contains two or three teeth per alveolus throughout much of the dental battery, although only one tooth is present in the anterior-most and posterior-most tooth families, neither of which appears to contribute to the occlusal surface. While the second tooth family from the anterior margin contains a single functional tooth, the rest of the tooth families contain two or three functional teeth. In nestling *M. peeblesorum*, there are up to three functional teeth per tooth family (Prieto-Márquez and Guenther 2018), while embryonic *H. stebingeri* possess a single functional tooth per family (Horner and Currie 1994).

The occlusal surface of the dentary teeth of CMN 8917 near the center of the tooth rows is concave, with a steeper lingual wear zone (LWZ) and shallower buccal wear zone (BWZ), similar to the dual-function (sensu Erickson et al. 2012) morphology of many adult hadrosaurids, which may have been used in both slicing and grinding of food material (Erickson et al. 2012). Near the mid-point of the dental battery, the LWZ reaches an angle of approximately 60° in relation to the horizontal, which transitions labially into the BWZ, the latter angled between 29° and 40° degrees from the horizontal. The angle between the LWZ and BWZ is therefore approximately 145°–154°, which is slightly above the 140° angle reported for adult *Brachylophosaurus canadensis* and *Edmontosaurus regalis* (Cuthbertson et al. 2012), but overlaps with the 150°–154° angles of adult *H. stebingeri* (Erickson and Zelenitsky 2014). The BWZ in CMN 8917 is less extensive and the transition between wear zones more gradual than in adult hadrosaurids, presumably the result of fewer teeth contributing to the occlusal surface. In embryonic and nestling *H. stebingeri*, the occlusal surface is angled a shallow 18°–20°, with elevated margins that form a cup-shaped topology on the surface of the single functional tooth per alveolus (Erickson and Zelenitsky 2014). By the subadult stage, the occlusal surface of *H. stebingeri* is planar or minimally concave and angled 25° (Erickson and Zelenitsky 2014), only developing the steeper dual-function morphology

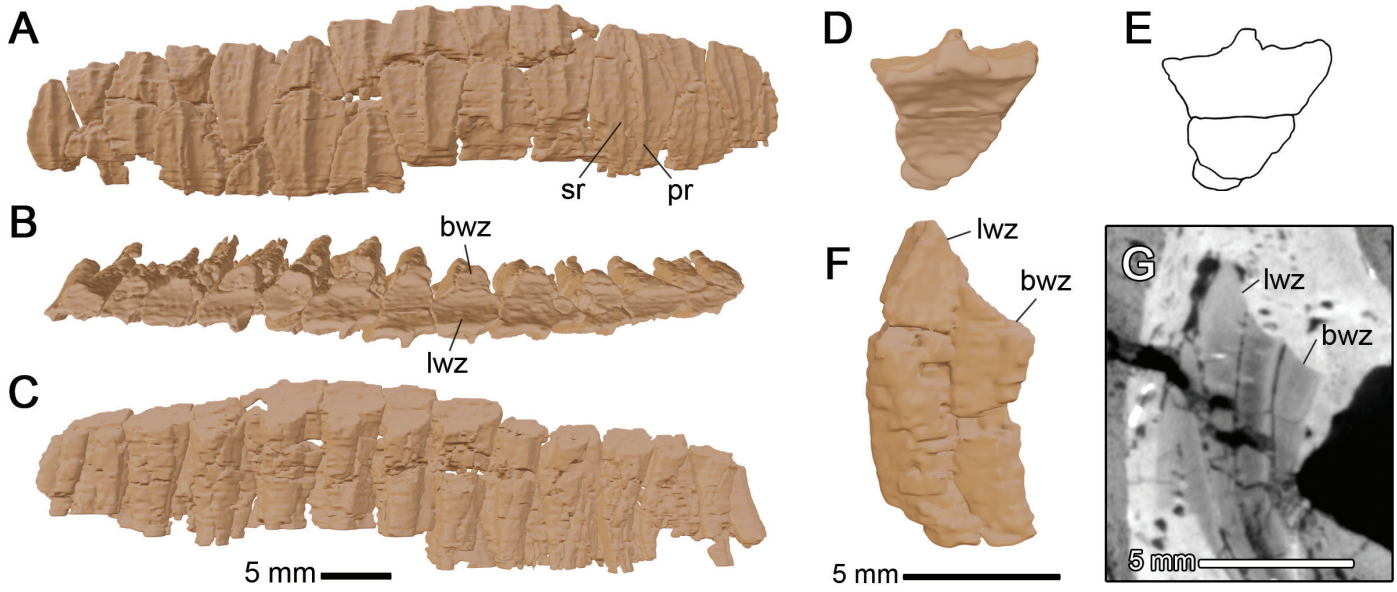

Figure 8. Right dentary dentition of CMN 8917. Dentary tooth rows (A–C) in A, lingual view; B, apical view; C, labial view; isolated dentary tooth family (eighth from anterior: D–F) in D, apical view; E, illustration of apical view highlighting individual teeth; F, distal view; G, frontal plane cross-section of dentary tooth family (ninth from anterior). Abbreviations: bwz, buccal worn zone; lwz, lingual worn zone; pr, primary ridge; sr, secondary ridge.

nearing adulthood. In *M. peeblesorum*, some nestlings are reported to possess cup-shaped occlusal surfaces similar to those of nestling *H. stebingeri* (Erickson and Zelenitsky 2014), while some nestling specimens—interpreted as large nestlings by Horner et al. (2000)—possess labiolingually concave occlusal surfaces angled approximately 60° (Prieto-Márquez and Guenther 2018), more akin to the morphology seen in CMN 8917. Given the more gradual transition between wear zones and less extensive BWZ compared to adult hadrosaurids, the occlusal surface of CMN 8917 may represent a transitional morphology between the shallow, cup-shaped surfaces of embryonic and small nestling hadrosaurids and the dual-function surfaces of many adults. The occlusal surface nearing the anterior and posterior regions of the tooth rows in CMN 8917 lacks distinct wear zones, is planar or mildly concave, and angled approximately 40° from the horizontal. The occlusal surface of hadrosaurids is known to vary across the anteroposterior length of the dental battery, although the anterior and posterior regions are generally more steeply inclined than the center (Horner et al. 2004). In tooth families with multiple functional teeth, the occlusal surface of CMN 8917 bears faint mesiodistal ridges that mark the shared edges of cohabiting teeth—the result of differential wear between different tissues—producing a complex topology that presumably aided in food processing (Erickson et al. 2012).

The dentary tooth crowns of CMN 8917 are lanceolate and have a height-to-width ratio of 2.0 near the mid-point of the dental battery. The angle between the tooth crowns and roots is approximately 130°, which falls within the values reported for hadrosaurines (between 120° and 140°) but below the >145° angles reported for lambeosaurines (Horner et al. 2004).

The enamel surface of the dentary tooth crowns of CMN 8917 possess prominent primary ridges located at the mesiodistal center of the tooth crowns. The primary ridges may be straight or slightly sinuous, the latter morphology being most prominent in the anterior-most tooth families. Some of the dentary teeth, most notably in the posterior tooth families, possess faint secondary ridges mesial to the primary ridges. Secondary ridges are traditionally associated with lambeosaurines (Horner et al. 2004; Prieto-Márquez et al. 2013; Fondevilla et al. 2018), but nestling *M. peeblesorum* (YPM-PU 22400) and juvenile *G. notabilis* (ROM 1939) can possess secondary ridges on their dentary teeth which are lost by adulthood (Prieto-Márquez and Guenther 2018; Mallon et al. 2022). Secondary ridges are also known from a juvenile *Edmontosaurus* sp. (DMNH 22851), on the dentary teeth of an adult *E. regalis* specimen (CMN 2289) (Takasaki et al. 2020), and infrequently on the dentary teeth of *Gryposaurus latidens* (Prieto-Márquez 2012), further highlighting the potential ontogenetic and individual variability of this trait.

DISCUSSION

The Taxonomy of CMN 8917

In the initial description of CMN 8917, Sternberg (1955) concluded that the specimen was a hadrosaurine, although his support for this assignment was not based on features currently understood as diagnostic at the subfamily level (Horner et al. 2004). Placement of CMN 8917 within Hadrosaurinae is, however, robustly supported by several features noted in this study: a narial vestibule not enclosed by the premaxillary dorsal and lateral processes, the presence of an anterodorsal process on the maxilla, and a maxillary dorsal process that is longer anteroposteriorly than dorsoventrally. Additionally, the crown-to-root angle of the dentary teeth of CMN 8917, here reported as 130°, falls within the range associated with hadrosaurines (Horner et al. 2004).

Other non-diagnostic features suggest hadrosaurine, and in some cases potential tribal, affinities. The anterolateral promontory on the maxilla is anteroposteriorly wide, as in kritosaurins (TMW-J, pers. obs.; Gates and Sampson 2007: fig. 7; Prieto-Márquez, 2012: fig. 5), brachylophosaurins (TMW-J, pers. obs.; Horner 1983: fig. 1), and saurolophins (TMW-J, pers. obs.), and is not pinched dorsally between the premaxilla and jugal as it is in lambeosaurines (TMW-J, pers. obs.; Horner et al. 2004; Evans 2010). The lateral surface of the mandibular ramus is convex with an apex that is ventral to the dorsoventral mid-height of the ramus, a morphology common in juvenile hadrosaurines (TMW-J, pers. obs.; Prieto-Márquez and Guenther, 2018: fig. 4D and H; Mallon et al. 2022: fig. 9), but that differs from juvenile lambeosaurines in which the apex is located at the approximate dorsoventral mid-height of the mandibular ramus (TMW-J, pers. obs.; Horner and Currie 1994: fig. 21.5; Farke et al. 2013: fig. 7). The ventral margin of the dentary, when viewed laterally, is subtly bowed anterior to the base of the coronoid process as in *Gryposaurus* spp. (TMW-J, pers. obs.; Prieto-Márquez 2012). This list of features highlights similarities between CMN 8917 and hadrosaurines, particularly kritosaurins, though it is unclear how variable some of these features would have been throughout hadrosaurid ontogeny.

Based on Sternberg's (1955) account of the fossil's location of origin, CMN 8917 would have come from well within Megaherbivore Assemblage Zone 1 (MAZ-1) of Mallon et al. (2012). Though multiple lambeosaurines occur in MAZ-1, *Gryposaurus notabilis* remains the only hadrosaurine known from this section of the DPF (Mallon et al. 2012; Lowi-Merri and Evans 2020: Table

1). This could make CMN 8917 the first and only nestling sized *Gryposaurus* specimen known to date, although given that the fossil lacks any diagnostic features of *Gryposaurus* (Gates and Sampson 2007; Prieto-Márquez 2012; Mallon et al. 2022), a generic identification is premature at this time.

The Taxonomic Value of Tooth Characters

Tooth characters, such as the presence of prominent denticles on the apical margins of the crowns and the presence of secondary ridges on the enamel surface of the crowns, were at one time used to support subfamilial affinities in hadrosaurids (Horner et al. 2004). Some recent studies, however, have called into question the utility of these features for taxonomic identification. Prominent marginal denticles are most common in lambeosaurines, but also occur in some kritosaurins (Horner et al. 2004; Prieto-Márquez 2012), while more diminutive ones occur in some brachylophosaurins (Prieto-Márquez and Guenther 2018). In the lambeosaurine *Hypacrosaurus stebingeri*, denticulation appears more prominent in embryonic rather than in nestling specimens (Horner and Currie 1994), suggesting ontogenetic variability in this trait, although it is unclear whether this is true of other taxa. Secondary ridges on the enamel surface of teeth, although commonly associated with lambeosaurines (Horner et al. 2004), occur in some nestling (Prieto-Márquez and Guenther 2018), juvenile (Takasaki et al. 2020; Mallon et al. 2022), and adult hadrosaurines (Prieto-Márquez 2012; Takasaki et al. 2020). In the case of *Maiasaura peeblesorum* and *Gryposaurus notabilis*, secondary ridges present in juvenile animals are absent in their adult counterparts (Prieto-Márquez and Guenther 2018; Mallon et al. 2022). The variability of these features throughout hadrosaurid ontogeny may represent the expression of ancestral traits during early development, as the aforementioned tooth characters are strongly expressed in non-hadrosaurid iguanodontians (Horner et al. 2004). It is unclear if these tooth characters would have changed throughout the ontogeny of CMN 8917, but their presence calls into question the use of these characters for subfamilial identification, given they are known from both subfamilies in at least some ontogenetic stages.

Ontogenetic Development in Hadrosaurines

The age of CMN 8917 cannot be directly determined, but the fossil is similar in size and dental battery morphology to specimens of *Maiasaura peeblesorum* (YPM-PU 22400) inferred to be large nestlings by Horner et al. (2000). The anteroposterior length of the maxilla of CMN 8917 is close to that reported for the YPM-PU 22400 specimens (Prieto-Márquez and Guenther 2018), and both CMN 8917 and YPM-PU 22400 have up to three functional teeth per alveolus in the dentary (Prieto-Márquez and Guenther 2018), which is more than in embryonic and nestling specimens of *Hypacrosaurus stebingeri* (Horner and Currie 1994). The steep, labiolingually concave occlusal surface of CMN 8917 resembles that of the large nestling YMP-PU 22400 specimens (Prieto-Márquez and Guenther 2018), differing from the shallow, cup-shaped occlusal surface of small nestling hadrosaurids from both subfamilies (Erickson and Zelenitsky 2014). Growth studies of *M. peeblesorum* suggest that the body size reached by skeletal maturity varied between individuals (Horner et al. 2000; Woodward et al. 2015). Using similarities in size between CMN 8917 and other specimens as evidence of similar age is, thus, not ideal, as it fails to consider inter- and intraspecific variation, but provides a best guess as to the ontogenetic stage of CMN 8917. Based on lines of arrested growth observed in the limb bones of *M. peeblesorum*, yearlings appear to have reached tibia lengths of above 50 cm (Horner et al. 2000; Woodward et al. 2015), well above the 12.5 cm average tibia length of the YPM-PU 22400 specimens (Prieto-Márquez and Guenther 2018). Being similar in size to the YPM-PU 22400 specimens, CMN 8917 falls well below the size reached by yearling *M. peeblesorum*, and, thus, would likely have been less than a year old, making it one of just a few hadrosaurines known from this early ontogenetic stage.

The occlusal surface of the dentary teeth of CMN 8917 varies across the tooth rows, with tooth families nearer the mid-point of the dental battery possessing a steep lingual wear zone (LWZ) and shallow buccal wear zone (BWZ). A similar dual-function morphology is present in many adult hadrosaurids that is thought to be the ancestral condition in Hadrosauridae (Erickson et al. 2012), but appears incompletely developed in CMN 8917, where the transition between wear zones is more gradual and the BWZ is less extensive than in adults. Therefore, the morphology of CMN 8917 may represent an intermediate stage between the shallow, cup-shaped occlusal surfaces of small nestling hadrosaurids (Erickson and Zelenitsky 2014) and the steeper dual-function morphology of many adults (Erickson et al. 2012; Erickson and Zelenitsky 2014).

The presence of a rudimentary dual-function occlusal surface in the early juvenile CMN 8917 contrasts with the ontogenetic changes known to have occurred in the lambeosaurine *H. stebingeri*, where dual-function dentition developed between the subadult and adult stages (Erickson and Zelenitsky 2014). This suggests differences in occlusal surface development between taxa. The cup-shaped occlusal surfaces of small nestling hadrosaurids may have been used to consume softer, succulent vegetation, while a dual-function morphology may have allowed adult hadrosaurids to consume tougher, fibrous vegetation (Erickson et al. 2012; Erickson and Zelenitsky 2014), the latter point supported

by studies of hadrosaurid coprolites (Chin 2007) and dental microwear patterns (Williams et al. 2009; Mallon and Anderson 2014). Differences in occlusal surface morphology between early-stage juveniles, thus, might reflect both developmental and dietary differences at an early age.

CONCLUSIONS

Juvenile material plays a key role in our understanding of hadrosaurid ontogeny (Horner et al. 2000; Erickson and Zelenitsky 2014; Prieto-Márquez and Guenther 2018; Mallon et al. 2022; Wyenberg-Henzler et al. 2022), and study of dental battery morphology in juvenile specimens can offer important insights into the early development of the hadrosaurid feeding apparatus (Erickson and Zelenitsky 2014). CMN 9817 represents one of only a few nestling-sized hadrosaurines known to date (Prieto-Márquez and Guenther 2018; Wosik et al. 2019), making it an important specimen. It shares several features diagnostic for the subfamily Hadrosaurinae, including the presence of a narial vestibule not enclosed within the premaxillary dorsal and lateral processes, an anterodorsal process on the maxilla, and a maxillary dorsal process that is longer anteroposteriorly than dorsoventrally. The presence of tooth characters traditionally associated with lambeosaurines, such as denticulated apical margins and secondary ridges on tooth crowns, reinforces prior suggestions that these characters are ontogenetically variable in some taxa, and, thus, may not be diagnostic in juvenile animals (Horner and Currie 1994; Prieto-Márquez and Guenther 2018; Takasaki et al. 2020; Mallon et al. 2022). The presence of a rudimentary dual-function occlusal surface at this early ontogenetic stage differs from the occlusal surface development described in the lambeosaurine *Hypacrosaurus stebingeri* (Erickson and Zelenitsky 2014), suggesting interspecific differences in dental battery development, potentially reflective of interspecific dietary differences during early ontogeny.

While ontogenetic changes in the occlusal surface of *H. stebingeri* are thoroughly described (Erickson and Zelenitsky 2014), it is unclear how this feature may have varied throughout the ontogeny of other taxa. Juvenile hadrosaurids from multiple genera are known (Waldman 1969; Dodson 1975; Horner and Currie 1994; Campione et al. 2013; Farke et al. 2013; Dewaele et al. 2015; Prieto-Márquez and Guenther 2018; Drysdale et al. 2019; Wosik et al. 2019; Takasaki et al. 2020; Mallon et al. 2022), offering an opportunity for future research to describe and compare occlusal surface morphology among various taxa at different ontogenetic stages. A better understanding of interspecific and ontogenetic differences in dental battery morphology could provide evidence for potential dietary shifts during ontogeny, and may provide insights into how multiple hadrosaurid taxa were apparently able to cohabit in Late Cretaceous environments like those represented by the DPF (see Mallon et al. 2012: fig. 1). This study highlights the importance of thoroughly studying juvenile specimens such as CMN 8917 with the aid of modern techniques to extract as much information as possible from these rare specimens. Though the Upper Cretaceous fossil record in North America may be imperfect, revisiting previously described specimens can still yield new information on the morphology and ontogeny of ancient animals, and help paint a better picture of organisms that inhabited the earth tens of millions of years ago.

ACKNOWLEDGEMENTS

A special thanks to Marissa Livius and Thomas Dudgeon for their help with 3D Slicer, Joshua Wasserlauf for feedback on an earlier version of this redescription, David C. Evans for having originally proposed CT scanning CMN 8917, and Philip J. Currie for looking into the stratigraphic origin of the specimen. We also wish to thank Brandon Strilisky, François Therrien, Scott Rufolo, and the staff of the RTMP and of the CMN for allowing and facilitating access to their collections. We would also like to acknowledge the Charlie Roots Honours Project Fund for financially supporting this research, and the Dale Patten Memorial Fund at the CMN for providing the computer used for 3D rendering CMN 8917. JCM is supported by a Natural Sciences and Engineering Research Council Discovery Grant (RGPIN-2017-06356).

LITERATURE CITED

Behrensmeyer, A.K., D. Western, and D.E. Dechant Boaz. 1979. New perspectives in vertebrate paleoecology from recent bone assemblage. Paleobiology 5:12–21. https://www.jstor.org/stable/2400386

Bell, P. R., and K. S. Brink. 2013. *Kazaklambia convincens* comb. nov., a primitive juvenile lambeosaurine from the Santonian of Kazakhstan. Cretaceous Research 45:265–274. DOI 10.1016/j.cretres.2013.05.003

Benson, R.B. 2018. Dinosaur macroevolution and macroecology. Annual Review of Ecology, Evolution, and Systematics 49:379–408. DOI 10.1146/annurev-ecolsys-110617-062231

Brown, C.M., D.C. Evans, N.E. Campione, L.J. O'Brien, and A.E. Eberth. 2013. Evidence for taphonomic size bias in the Dinosaur Park Formation (Campanian, Alberta), a model Mesozoic terrestrial alluvial-paralic system. Palaeogeography, Palaeoclimatology, Palaeoecology 372:108–122. DOI 10.1016/j.palaeo.2012.06.027

Brown, C.M., N.E. Campione, G.P. Wilson Mantilla, and D.C. Evans. 2022. Size-driven preservational and macroecological

biases in the latest Maastrichtian terrestrial vertebrate assemblages of North America. Paleobiology 48:210–238. DOI 10.1017/pab.2021.35

Campione, N.E., K.S. Brink, E.A. Freedman, C.T. McGarrity, and D.C. Evans. 2013. '*Glishades ericksoni*', an indeterminate juvenile hadrosaurid from the Two Medicine of Montana: implications for hadrosauroid diversity in the latest Cretaceous (Campanian-Maastrichtian) of western North America. Palaeobiodiversity and Palaeoenvironments 93:65–75. DOI 10.1007/s12549-012-0097-1

Case, J.A, J.E. Martin, D.S. Chaney, R. Marcelo, M.O. Woodburne, and J.M. Parrish. 1998. The first hadrosaur from Antarctica. Journal of Vertebrate Paleontology 18:32.

Chin, K. 2007. The paleobiological implications of herbivorous dinosaur coprolites from the Upper Cretaceous Two Medicine Formation of Montana: why eat wood? PALAIOS 22:554–566. https://www.jstor.org/stable/27670548

Currie, P. J. 2005. History of research; pp. 3–33 in P.J. Currie and E.B. Koppelhus (eds.), Dinosaur Provincial Park: A Spectacular Ancient Ecosystem Revealed. Indiana University Press, Bloomington, Indiana, United States of America.

Cuthbertson, R., and R.B. Holmes. 2010. The first complete description of the holotype of *Brachylophosaurus canadensis* Sternberg, 1953 (Dinosauria: Hadrosauridae) with comments on intraspecific variation. Zoological Journal of the Linnaean Society 159:373–397.

Cuthbertson, R.S., A. Tirabasso, N. Rybczynski, and R.B. Holmes. 2012. Kinetic limitations of intracranial joints in *Brachylophosaurus canadensis* and *Edmontosaurus regalis* (Dinosauria: Hadrosauridae), and their implications for the chewing mechanics of hadrosaurids. Anatomical Record 295:968–979.

Dewaele, L., K. Tsogtbaatar, R. Barsbold, G. Garcia, K. Stein, F. Escuillié, and P. Godefroit. 2015. Perinatal specimens of *Saurolophus angustirostris* (Dinosauria: Hadrosauridae), from the Upper Cretaceous of Mongolia. PLoS ONE 10(10), e0128806. DOI 10.1371/journal.pone.0138806

Dodson, P. 1975. Taxonomic implications of relative growth in lambeosaurine hadrosaurs. Systematic Zoology 24:37–54. https://www.jstor.org/stable/2412696

Drysdale, E.T., F. Therrien, D.K. Zelenitsky, D.B. Weishampel, and D.C. Evans. 2019. Description of juvenile specimens of *Prosaurolophus maximus* (Hadrosauridae, Saurolophinae) from the Upper Cretaceous Bearpaw Formation of southern Alberta, Canada, reveals ontogenetic changes in crest morphology. Journal of Vertebrate Paleontology 38, e1547310. DOI 10.1080/02724634.2018.1547310

Eberth, D.A., and P.J. Currie. 2005. Vertebrate taphonomy and taphonomic modes; pp. 453–477 in P.J. Currie and E.B. Koppelhus (eds.), Dinosaur Provincial Park: a Spectacular Ancient Ecosystem Revealed. Indiana University Press, Bloomington, Indiana United States of America.

Eberth, D.A., M. Shannon, and B.C. Noland. 2007. A bonebeds database: classification, biases, and patterns of occurrences; pp. 103–220 in R.R. Rogers, D.A. Eberth, and A.R. Fiorillo (eds.), Bonebeds: Genesis, Analysis, and Paleobiological Significance. University of Chicago Press, Illinois, USA. DOI 10.7208/chicago/9780226723730.003.0003

Edmund, A.G. 1957. On the special foramina in the jaws of many ornithischian dinosaurs. Contributions of the Royal Ontario Museum Division of Zoology and Paleontology 48:3–14.

Erickson, G.M., and D. Zelenitsky. 2014. Osteohistology and occlusal morphology of *Hypacrosaurus stebingeri* teeth throughout ontogeny with comments on wear-induced form and function; pp. 422–432 in D.A. Eberth and D.C. Evans (eds.), Hadrosaurs. Indiana University Press, Bloomington, Indiana, Unites States of America.

Erickson, G.M., B.A. Krick, M. Hamilton, G.R. Bourne, M.A. Norell, E. Lilleodden, and W.G. Sawyer. 2012. Complex dental structure and wear biomechanics in hadrosaurid dinosaurs. Science 228:98–101. DOI 10.1126/science.1224495

Evans, D.C. 2010. Cranial anatomy and systematics of *Hypacrosaurus altispinus*, and a comparative analysis of skull growth in lambeosaurine hadrosaurids (Dinosauria: Ornithischia). Zoological Journal of the Linnean Society 159:398–434.

Farke, A.A., D.J. Chok, A. Herrero, B. Scolieri, and S. Werning. 2013. Ontogeny in the tube-crested dinosaur *Parasaurolophus* (Hadrosauridae) and heterochrony in hadrosaurids. PeerJ. DOI 10.7717/peerj.182

Fastovsky, D.E., A. Bercovici, B. Vila, J. O. Oms, J. Dinares-Turell, and J. Marmi. 2016. The Hell Creek Formation and its contribution to the Cretaceous–Paleogene extinction; a short primer. Cretaceous Research 57:368–390. DOI 10.1016/j.cretres.2015.07.007

Federov, A., R. Beichel, J. Kalpathy-Cramer, J. Finet, J-C. Fillion-Robin, S. Pujol, C. Bauer, D. Jennings, F.M. Fennessy, M. Sonka, J. Buatti, S.R. Aylward, J.V. Miller, S. Pieper, and R. Kikinis. 2021. 3D Slicer as an image computing platform for the quantitative imaging network. Magnetic Resonance Imaging 30(9):1323–1341. DOI 10.1016/j.mri.2012.05.001

Fondevilla, V., F.M. Dalla Vecchia, R. Gaete, A. Galobart, B. Moncunill-Solé, and M. Köhler. 2018. Ontogeny and taxonomy of the hadrosaur (Dinosauria, Ornithopoda) remains from Basturs Poble bonebed (late early Maastrichtian, Tremp syncline, Spain). PLoS ONE 13(10). DOI 10.1371/journal.pone.0206287

Freedman Fowler, E., and J. R. Horner. 2015. A new brachylophosaurin hadrosaur (Dinosauria: Ornithischia) with an intermediate nasal crest from the Campanian Judith River Formation of northcentral Montana. PLoS ONE 10:e141304. DOI 10.1371/journal.pone.0141304

Galton, P.M. 1973. The cheeks of ornithischian dinosaurs. Lethaia 6:67–89.

Gates, T.A., and S.D. Sampson. 2007. A new species of *Gryposaurus* (Dinosauria: Hadrosauridae) from the late Campanian Kaiparowits Formation, southern Utah, USA. Zoological Journal of the Linnaean Society 151:351–376.

Hone, D. W. E., A. F. Farke, and M. J. Wedel. 2016. Ontogeny and the fossil record: what, if anything, is an adult dinosaur? Biology Letters 12:20150947. DOI 10.1098/rsbl.2015.0947

Horner, J. R. 1983. Cranial osteology and morphology of the type specimen of *Maiasaura peeblesorum* (Ornithischia: Hadrosauridae), with discussion of its phylogenetic position. Journal of Vertebrate Paleontology 3:29–38.

Horner, J.R. 1992. Cranial morphology of *Prosaurolophus* (Ornithischia: Hadrosauridae) with descriptions of two new hadrosaurid species and an evaluation of hadrosaurid phylogenetic relationships. Museum of the Rockies Occasional Paper no. 2:1–119.

Horner, J.R., and R. Makela. 1979. Nest of juveniles provides evidence of family structure among dinosaurs. Nature 282:296–298. DOI 10.1038/282296a0

Horner, J.R., and P.J. Currie. 1994. Embryonic and neonatal morphology and ontogeny of a new species of *Hypacrosaurus* (Ornithischia, Lambeosauridae) from Montana and Alberta; pp. 312–336 in K. Carpenter, K.F. Hirsch, and J.R. Horner (eds.), Dinosaur Eggs and Babies. Cambridge University Press, New York.

Horner, J.R., A. De Ricqlès, and K. Padian. 2000. Long bone histology of the hadrosaurid dinosaur *Maiasaura peeblesorum*: growth dynamics and physiology based on an ontogenetic series of skeletal elements. Journal of Vertebrate Paleontology 20:115–129.

Horner, J.R., D.B. Weishampel, and C.A. Forster. 2004. Hadrosauridae; pp. 438–463 in D.B. Weishampel, P. Dodson, and H. Osmólska (eds.), The Dinosauria, 2nd edition. University of California Press Ltd, London, UK.

Horner, J.R., M.B. Goodwin, and N. Myhrvold. 2011 Dinosaur census reveals abundant *Tyrannosaurus* and rare ontogenetic stages in the Upper Cretaceous Hell Creek Formation (Maastrichtian), Montana, USA. PLoS ONE 6(2), e16574. DOI 10.1371/journal.pone.0016574

Longrich, N.R., X.P. Suberbiola, R.A. Pyron, and N. Jalil. 2021. The first duckbill dinosaur (Hadrosauridae: Lambeosaurinae) from Africa and the role of oceanic dispersal in dinosaur biogeography. Cretaceous Research 120:104678. DOI 10.1016/j.cretres.2020.104678

Lowi-Merri, T.M., and D.C. Evans. 2020. Cranial variation in *Gryposaurus* and biostratigraphy of hadrosaurines (Ornithischia: Hadrosauridae) from the Dinosaur Park Formation of Alberta, Canada. Canadian Journal of Earth Sciences 57:765–779. dx.doi.org/10.1139/cjes-2019-0073

Lull, R.S., and N.E. Wright. 1942. Hadrosaurian dinosaurs of North America. Geological Society of America Special Papers 40, 242 pp.

Mallon, J.C., D.C. Evans, M.J. Ryan, and J.S. Anderson. 2012. Megahervivorous dinosaur turnover in the Dinosaur Park Formation (upper Campanian) of Alberta, Canada. Palaeogeography, Palaeoclimatology, Palaeoecology 350:124–138. DOI 10.1016/j.palaeo.2012.06.024

Mallon, J.C., and J.S. Anderson. 2014. The functional and palaecological implications of tooth morphology and wear for the megaherbivorous dinosaurs from the Dinosaur Park Formation (upper Campanian) of Alberta, Canada. PLoS ONE 9(6), e98605. DOI 10.1371/journal.pone.0098605

Mallon, J.C., D.C. Evans, Y. Zhang, and H. Xing. 2022. Rare juvenile material constrains estimation of skeletal allometry in *Gryposaurus notabilis* (Dinosauria: Hadrosauridae). Anatomical Record. DOI 10.1002/ar.25021

McGarrity, C.T., N.E. Campione, and D.C. Evans. 2013. Cranial anatomy and variation in *Prosaurolophus maximus* (Dinosauria: Hadrosauridae). Zoological Journal of the Linnaean Society 167:531–568. DOI 10.1111/zoj.12009

Prieto-Márquez, A. 2010. Global historical biogeography of hadrosaurid dinosaurs. Zoological Journal of the Linnean Society 159:503–525.

Prieto-Márquez, A. 2012. The skull and appendicular skeleton of *Gryposaurus latidens*, a saurolophine hadrosaurid (Dinosauria: Ornithopoda) from the early Campanian (Cretaceous) of Montana, USA. Canadian Journal of Earth Sciences 49:510–532.

Prieto-Márquez, A. 2014. Skeletal morphology of *Kritosaurus navajovius* (Dinosauria: Hadrosauridae) from the Late Cretaceous of the North American south-west, with an evaluation of the phylogenetic systematics and biogeography of Kritosaurini. Journal of Systematic Palaeontology 12:133–175. DOI 10.1080/14772019.2013.770417

Prieto-Márquez, A., F.M. Dalla Vecchia, R. Gaete, and À. Galobart. 2013. Diversity, relationships, and biogeography of the lambeosaurine dinosaurs from the European archipelago, with description of the new aralosaurin *Canardia garonnensis*. PLoS ONE 8, e69835. DOI 10.1371/journal.pone.0069835

Prieto-Márquez, A., G. M. Erickson, and J. A. Eversole. 2016. A primitive hadrosaurid from southeastern North America and the origins and early evolution of 'duck-billed' dinosaurs. Journal of Vertebrate Paleontology 36:e1054495. DOI 10.1080/02724634.2015.1054495

Prieto-Márquez, A., and M.F. Guenther. 2018. Perinatal specimens of *Maiasaura* from the Upper Cretaceous of Montana (USA): insights into the early ontogeny of saurolophine hadrosaurid dinosaurs. Peer J 6. DOI 10.7717/peerj.4734

Ramezani, J., T.L. Beveridge, R.R. Rogers, D.A. Eberth, and E.M. Roberts. 2022. Calibrating the zenith of dinosaur diversity in the Campanian of the Western Interior Basin by CA-ID-TIMS U-Pb geochronology. Scientific Reports 12:16026. DOI 10.1038/s41598-022-19896-w

Smith, J.B., and P. Dodson. 2003. A proposal for a standard terminology of anatomical notation and orientation in fossil vertebrate dentitions. Journal of Vertebrate Paleontology 23:1–12. DOI 10.1671/0272-4634(2003)23[1:APFAST]2.0.CO;2

Sternberg, C.M. 1955. A juvenile hadrosaur from the Oldman Formation of Alberta. National Museum of Canada Bulletin 136:120–122.

Stubbs, T.L., M.J. Benton, A. Esler, and A. Prieto-Márquez. 2019. Morphological innovation and the evolution of hadrosaurid dinosaurs. Paleobiology 45:347–362. DOI 10.1017/pab.2019.9

Takasaki, R., A.R. Fiorillo, R.S. Tykoski, and Y. Kobayashi. 2020. Re-examination of the cranial osteology of the Arctic Alaskan hadrosaurine with implications for its taxonomic status. PLoS ONE 15, e0232410. DOI 10.1371/journal.pone.0232410

Wagner, J., and Lehman, T.M. 2009. An enigmatic new lambeosaurine hadrosaur (Reptilia: Dinosauria) from the Upper Shale member of the Campanian Aguja Formation of Trans-Pecos Texas. Journal of Vertebrate Paleontology 29:605–611. DOI 10.1671/039.029.0208

Waldman, M. 1969. On an immature specimen of *Kritosaurus notabilis* (Lambe), (Ornithischia: Hadrosauridae) from the Upper Cretaceous of Alberta, Canada. Canadian Journal of Earth Sciences 6:569–576.

Weishampel, D.B. 1984. Evolution of jaw mechanics in ornithopod dinosaurs. Advances in Anatomy, Embryology, and Cell Biology 87:1–109.

Williams, V.S., P.M. Barrett, and M.A. Purnell. 2009. Quantitative analysis of dental microwear in hadrosaurid dinosaurs, and the implications for hypotheses of jaw mechanics. Proceedings in the National Academy of Sciences 106:11194–11199. DOI 10.1073/pnas.0812631106

Woodward, H.N., E. Freedman Fowler, J.O. Farlow, and J.R. Horner. 2015. *Maiasaura*, a model organism for extinct vertebrate population biology: a large sample statistical assessment of growth dynamics and survivorship. Paleobiology 41:503–527. https://www.jstor.org/stable/44017947

Wosik, M., M.B. Goodwin, and D.C. Evans. 2019. Nestling-sized hadrosaurine cranial material from the Hell Creek Formation of northeastern Montana, USA, with an analysis of cranial ontogeny in *Edmontosaurus annectens*. PaleoBios 36. DOI 10.5070/P9361044525

Wyenberg-Henzler, T., R.T. Patterson, J.C. Mallon. 2022. Ontogenetic dietary shifts in North American hadrosaurids (Dinosauria: Ornithischia). Cretaceous Research 135:105177. DOI 10.1016/j.cretres.2022.105177

Xing, H., J.C. Mallon, and M.L. Currie. 2017. Supplementary cranial description of the types of *Edmontosaurus regalis* (Ornithischia: Hadrosauridae), with comments on the phylogenetics and biogeography of Hadrosaurinae. PLoS ONE 12, e175253. DOI 10.1371/journal.pone.0175253

Appendix 1. Comparative material used in the description of CMN 8917.

Specimen number	Taxon	Ontogenetic stage	Sources
CMN 8893	*Brachylophosaurus canadensis*	Adult	TMW-J, pers. obs.; Cuthbertson and Holmes 2010
CMN 8503, CMN 8676, and CMN 8704	*Corythosaurus casuarius*	Adults	TMW-J, pers obs.
CMN 36141	*Corythosaurus casuarius*	Juvenile	TMW-J, pers. obs.
CMN 8509	*Edmontosaurus annectens*	Adult	TMW-J, pers. obs.
UCMP 235860	*Edmontosaurus* cf. *E. annectens*	Nestling	Wosik et al. 2019
CMN 2288 and CMN 2289	*Edmontosaurus regalis*	Adults	TMW-J, pers. obs.; Xing et al. 2017; Takasaki et al. 2020
DMNH 22851	*Edmontosaurus* sp.	Juvenile	Takasaki et al. 2020
AMNH FARB 5465 and MOR 478-5-28-8-1	*Gryposaurus latidens*	Adults	Prieto-Márquez 2012
RAM 6797	*Gryposaurus monumentensis*	Adult	Gates and Sampson 2007
CMN 2278	*Gryposaurus notabilis*	Adult	TMW-J, pers. obs.
CMN 8784 and ROM 1939	*Gryposaurus notabilis*	Juveniles	TMW-J, pers. obs.; Waldman 1969; Mallon et al. 2022
CMN 8501, CMN 8673, and ROM 702	*Hypacrosaurus altispinus*	Adults	TMW-J, pers. obs.; Evans 2010
CMN 2247	*Hypacrosaurus altispinus*	Juvenile	TMW-J, pers. obs.
TMP 1988.151.88 TMP 1994.666.80, and TMP 1994.385.1	*Hypacrosaurus stebingeri*	Juveniles	TMW-J, pers. obs.; Horner and Currie 1994
TMP 1987.79.266, TMP 1987.79.334 TMP 1987.79.336, and TMP 1989.79.52	*Hypacrosaurus stebingeri*	Embryos and nestlings	Horner and Currie 1994

Appendix 1, continued. Comparative material used in the description of CMN 8917.

AMNH 5799 and USNM 8629	*Kritosaurus navajovius*	Adult	Prieto-Márquez 2014
CMN 8703	*Lambeosaurus clavinitialis*	Adult	TMW-J, pers. obs.
CMN 8705 and TMP 1966.4.1	*Lambeosaurus magnicristatus*	Adult	TMW-J, pers. obs.
PU 22405	*Maiasaura peeblesorum*	Adult	Horner 1983
YPM-PU 22400	*Maiasaura peeblesorum*	Nestlings	Horner et al. 2000; Prieto-Márquez and Guenther 2018
RAM 14000	*Parasaurolophus* sp.	Juvenile	Farke et al. 2013
MOR 454 and MOR 447	*Prosaurolophus maximus*	Adult	Horner 1992
CMN 2277, CMN 2870, TMP 1984.1.1, and ROM 787	*Prosaurolophus maximus*	Adults	TMW-J, pers. obs.; McGarrity et al. 2013
TMP 1983.64.3, TMP 1998.50.1, and TMP 2016.37.1	*Prosaurolophus maximus*	Juveniles	TMW-J, pers. obs.; Drysdale et al. 2019
MPC-D100/764	*Saurolophus angustirostris*	Nestlings	Dewaele et al. 2015
CMN 8796	*Saurolophus osborni*	Adult	TMW-J, pers. obs.